Hyperspectral Image Denoising With a Spatial–Spectral View Fusion Strategy

Qiangqiang Yuan, Liangpei Zhang, *Senior Member, IEEE*, and Huanfeng Shen, *Senior Member, IEEE*

***Abstract*— In this paper, we propose a hyperspectral image denoising algorithm with a spatial–spectral view fusion strategy. The idea is to denoise a noisy hyperspectral 3-D cube using the hyperspectral total variation algorithm, but applied to both the spatial and spectral views. A metric Q-weighted fusion algorithm is then adopted to merge the denoising results of the two views together, so that the denoising result is improved. A number of experiments illustrate that the proposed approach can produce a better denoising result than both the individual spatial and spectral view denoising results.**

***Index Terms*— Hyperspectral image denoising, spatial view, spectral view, total variation.**

I. Introduction

HYPERSPECTRAL images, with abundant spectral information, have been widely used to distinguish different land-cover types, which is very important for detecting minerals, urban planning, etc. [1], [2]. Unfortunately, because there are a number of limitations with both the theoretical and sensor aspects, a hyperspectral image will be contaminated with some noise, which not only influences the visual effect but also decreases the precision of the subsequent processing. It is therefore important to reduce the noise in the hyperspectral image.

In the past decades, the hyperspectral image denoising problem has been explored by many researchers. The approaches to the problem can be classified into four groups. The first group is the subspace-based methods. The most popular method is principal component analysis (PCA) denoising, which retains the first few principal components (PCs) containing most of the information and discards the rest of the PCs which contain little information and are assumed to be noise. Finally, the denoised image is reconstructed from the high-rank PCs.

Manuscript received February 3, 2013; revised March 24, 2013; accepted April 17, 2013. Date of publication July 15, 2013; date of current version February 27, 2014. This work was supported in part by the Major State Basic Research Development Program (973 Program) of China under Grant 2011CB707103, the National Natural Science Foundation of China under Grant 40930532, Grant 41271376, and Grant 61102128, the National Science and Technology Support Program under Grant 2012BAJ23B03, and the China Postdoctoral Science Foundation under Grant 2012M521471.

Q. Yuan is with the School of Geodesy and Geomatics, Wuhan University, Wuhan 430079, China (e-mail: yqiang86@gmail.com).

L. Zhang is with the State Key Laboratory of Information Engineering in Surveying, Mapping, and Remote Sensing, Wuhan University, Wuhan 430079, China (e-mail: zlp62@whu.edu.cn).

H. Shen is with the School of Resource and Environmental Science, Wuhan University, Wuhan 430079, China (e-mail: shenhf@whu.edu.cn).

Color versions of one or more of the figures in this paper are available online at http://ieeexplore.ieee.org.

Digital Object Identifier 10.1109/TGRS.2013.2259245

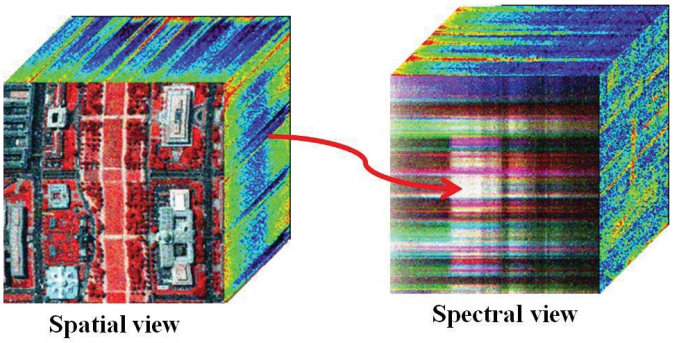

Fig. 1. Spatial and spectral views in a hyperspectral image.

However, although the first few PCs contain the most information, there will still be some noise remaining in them, and it is also possible that some useful information will be included in the low-rank PCs. To address these issues, some other subspace-based selection methods have been developed [3]–[5]. The second group is wavelet-based algorithms, such as the hybrid spatial–spectral derivative-domain wavelet shrinkage noise reduction (HSSNR) approach proposed by Othman and Qian [6]. Recently, Chen *et al.* [7] proposed a new hyperspectral image denoising algorithm by adding a PCA transform before using wavelet shrinkage. In this approach, a PCA transform is first implemented on the original hyperspectral image, and then the low-energy PCA output channel is denoised with a wavelet shrinkage denoising process. This method performs very well when the noise level of the data cubes is relatively low. Another group of algorithms is based on the tensor decomposition method [8]–[11], in which a hyperspectral image is represented by a tensor model and is separated with a tensor decomposition method such as the Tucker3 [8] or parallel factor analysis (PARAFAC) [9]. The last group of algorithms is the partial differential equation (PDE) based methods. These include the hyperspectral anisotropic diffusion model proposed by Martín-Herrero *et al.* [12], [13], and the improved anisotropic diffusion model in [14] and [15]. In [16], a spatial–spectral adaptive hyperspectral total variation denoising method was proposed that can adjust the denoising strength both across and between the bands.

A hyperspectral image is usually viewed from the front, which is the spatial view. However, a hyperspectral image, if viewed from the side direction, will also have a spectral view, which is shown in Fig. 1. For a hyperspectral image, noise not only exists in the spatial view but also in the spectral view (Fig. 2). In most hyperspectral image denoising methods,

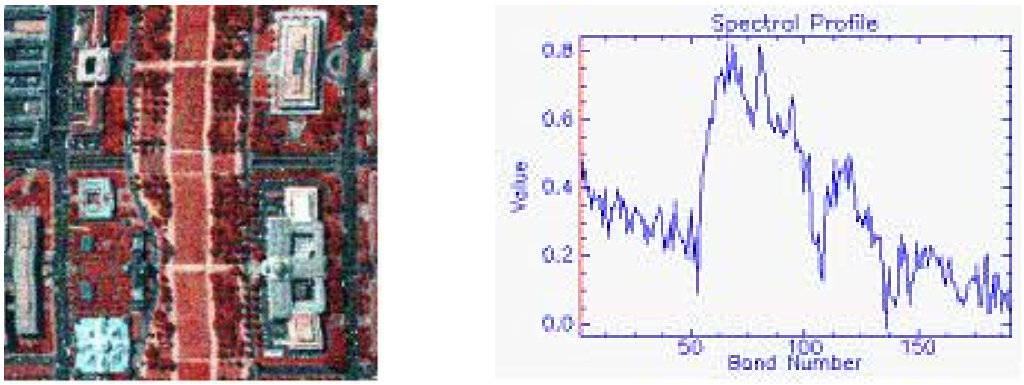

(a) Spatial view noise **(b) Spectral view noise**

Fig. 2. Noise existing in both the spatial view and the spectral view in a hyperspectral image.

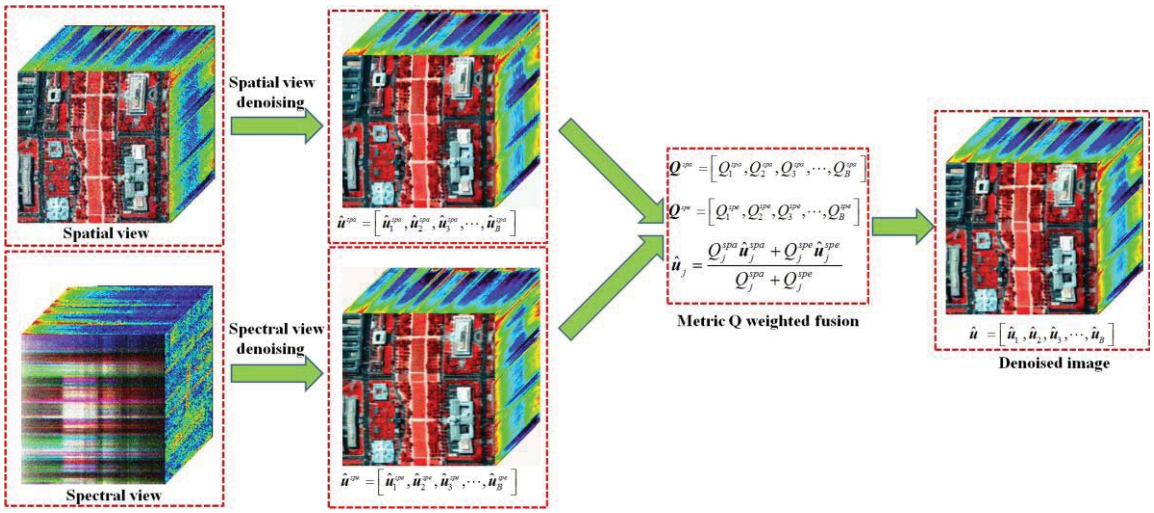

Fig. 3. Flowchart of the proposed spatial–spectral view fusion algorithm.

the hyperspectral image is just denoised from the spatial view, ignoring the role of the spectral view. Therefore, in this paper, we propose a spatial–spectral view fusion algorithm for hyperspectral image denoising. A noisy hyperspectral image is first denoised using the hyperspectral total variation (TV) approach proposed in our previous work [16], from both the spatial and spectral views, and then the denoising results of the two views are fused using a metric Q-weighting strategy. A flowchart of the proposed algorithm is shown in Fig. 3.

The remainder of this paper is organized as follows: In Section II, the hyperspectral image TV denoising model is presented. In Section III, the spatial–spectral view fusion strategy is introduced in detail. The experimental results and a discussion are presented in Section IV. Finally, the conclusion is given in Section V.

II. Hyperspectral Total Variation Denoising

A. Regularized Hyperspectral Denoising Model

Assuming that we have an original hyperspectral image, and the degradation noise is assumed to be additive and random distributed noise, the noise degradation model of the hyperspectral image can be written as

$$f = u + n \tag{1}$$

where $u = [u_1, u_2, \ldots, u_j, \ldots, u_B]$ is the clear hyperspectral image, with the size $M \times N \times B$, in which M represents the samples of each band in the whole image, N stands for the lines of the image, and B is the number of bands. $f = [f_1, f_2, \ldots, f_j, \ldots, f_B]$ is the noise degradation image, which is also of size $M \times N \times B$, and $n = [n_1, n_2, \ldots, n_j, \ldots, n_B]$ is the additive noise with the same size as u and f. In this paper, we assume that the noise n is independent of the signal u.

The denoising model for a hyperspectral image can be represented as the following regularization-based problem [16]:

$$\hat{u} = \arg\min \left\{ \sum_{j=1}^{B} \left\| u_j - f_j \right\|_2^2 + \lambda R(u) \right\}. \tag{2}$$

In (2), $\sum_{j=1}^{B} \left\| u_j - f_j \right\|_2^2$ is the data fidelity item, which stands for the fidelity between the observed noisy image and the original clear image, and $R(u)$ is the regularization item, which gives a prior model of the original clear hyperspectral

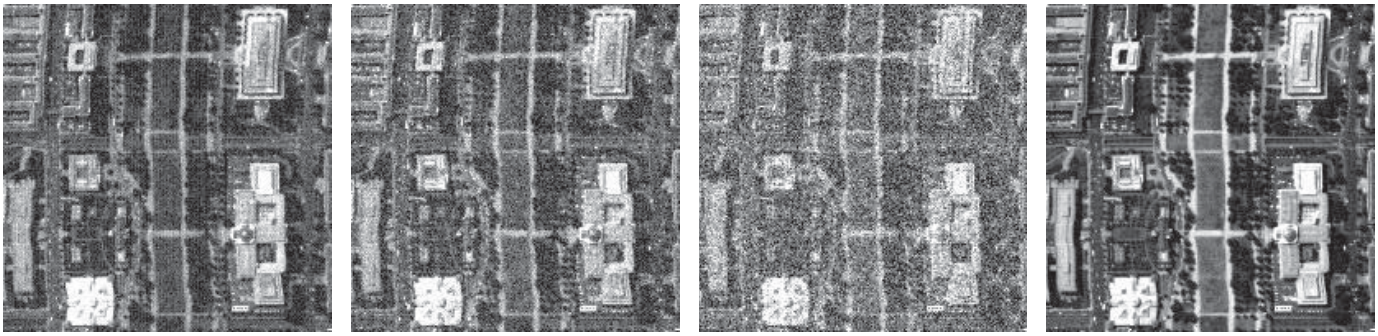

Fig. 4. Noise distribution in the spatial views. (a) Band 1. (b) Band 10. (c) Band 20. (d) Band 30.

image u. λ is the regularization parameter, which controls the relative contribution between the data fidelity and the regularization item.

The prior model of the hyperspectral image $R(u)$ plays a very important role in the process of denoising. It controls the perturbation of the solution and solves the ill-posed problem [17]. Based on the regularization theory, many regularization models have been proposed, including the Laplacian regularization [18], Gaussian–Markov random fields model [19], TV regularization [20], manifold regularization [21], and divergence-based regularization [22]. Among these models, TV regularization is very effective because of its strong ability of edge preservation, and it has been widely used in image deblurring [23], super-resolution [24], [25], and text decomposition [26]. Based on the single band TV model, a spectral–spatial adaptive hyperspectral TV model is proposed in [16], which will be introduced in the next part.

B. Hyperspectral Total Variation (TV) Model

For a gray-level image u, the TV model is defined as follows:

$$R(u) = TV(u) = \sum_i \sqrt{\left(\nabla_i^h u\right)^2 + \left(\nabla_i^v u\right)^2} \tag{3}$$

where ∇_i^h and ∇_i^v are linear operators corresponding to the horizontal and vertical first-order differences, respectively, at pixel i. $\nabla_i^h u = u_i - u_{r(i)}$ and $\nabla_i^v u = u_i - u_{b(i)}$, where $r(i)$ and $b(i)$ represent the nearest neighbors to the right of and below the pixel.

In [16], we define two hyperspectral TV models, which have the following formulations:

$$\mathrm{HTV}_1(u) = \sum_{i=1}^{MN} \sqrt{\sum_{j=1}^{B} (\nabla_{ij} u)^2} \tag{4}$$

$$\mathrm{HTV}_2(u) = \sum_{i=1}^{MN} W_i \sqrt{\sum_{j=1}^{B} (\nabla_{ij} u)^2} \tag{5}$$

$$G = \sqrt{\sum_{j=1}^{B} \left(\nabla u_j\right)^2} \quad \tau_i = \frac{1}{1 + \mu G_i}$$

$$W_i = \frac{\tau_i}{\bar{\tau}} \quad \bar{\tau} = \frac{\sum_{i=1}^{MN} \tau_i}{MN} \tag{6}$$

where MN is the total number of pixels in one hyperspectral band, and B is the total number of bands. ∇_{ij} are linear operators corresponding to the first-order differences at the ith pixel in the jth band, respectively. ∇u_j is the gradient map of the jth band. G means the gradient information of every band is added together and the square root is taken of each element of the sum. W_i is a weighting parameter to control the regularization strength in the different pixels.

The first model in (4) is called the spectral adaptive hyperspectral TV model, which can give consideration to the noise distribution characteristic of the hyperspectral image and automatically adjust the denoising strength in different spectral bands with the noise intensity. In high noise intensity bands, a strong denoising strength will be used, while in low noise intensity bands a weak strength will be used. The second model in (5) is called the spectral–spatial adaptive TV model, which can not only adaptively adjust the denoising strength in the different spectral bands, in the same way as the spectral adaptive model, but can also constrain the denoising strength in different pixels, with the help of the spatial information parameter W_i. For the pixels in flat regions, a strong regularization strength is enforced to suppress noise and, conversely, a weak regularization strength is enforced on the edge pixels to preserve them.

III. Spatial–Spectral View Denoising and Fusion

A. Spatial and Spectral View Denoising

As mentioned in the introduction, a hyperspectral image has both spatial and spectral views, and the noise distribution in the two views will be different. In the following section, the differences are presented and analyzed. After this, we show how to use the hyperspectral TV models on the two views.

For a hyperspectral image, the noise intensity in each band varies. In the following figures, using the DC Mall image as an example, we randomly add noise of different intensity to the different bands and present the noise distribution differences in the two views. Fig. 4 shows the noise distribution in the spatial views, and Fig. 5 presents the noise distribution in the spectral views. From the two sets of figures, it can be seen that the noise distribution in the spatial views is different from the distribution in the spectral views. In the spatial view, the noise intensity in each band is different, while, if the spatial view is transformed to a spectral view, it will appear that

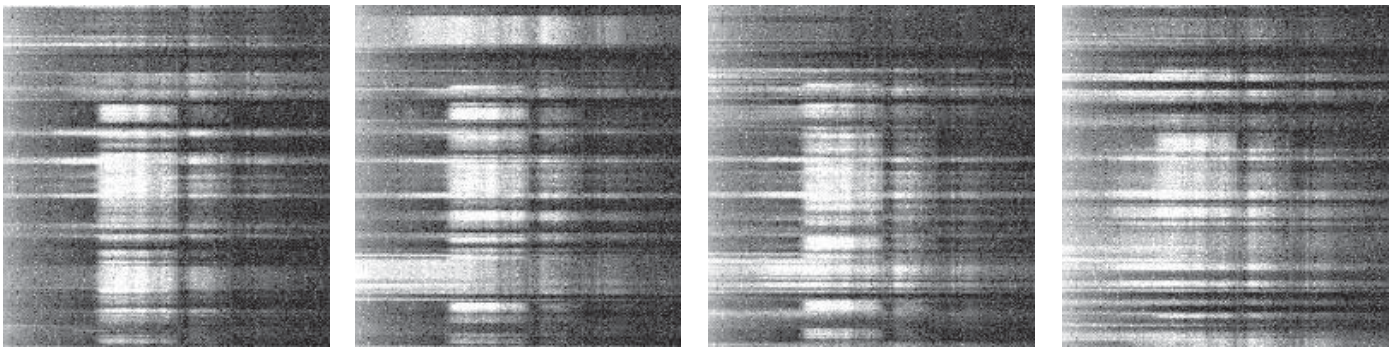

(a) (b) (c) (d)

Fig. 5. Noise distribution in the spectral views. (a) Band 1, (b) Band 10. (c) Band 20. (d) Band 30.

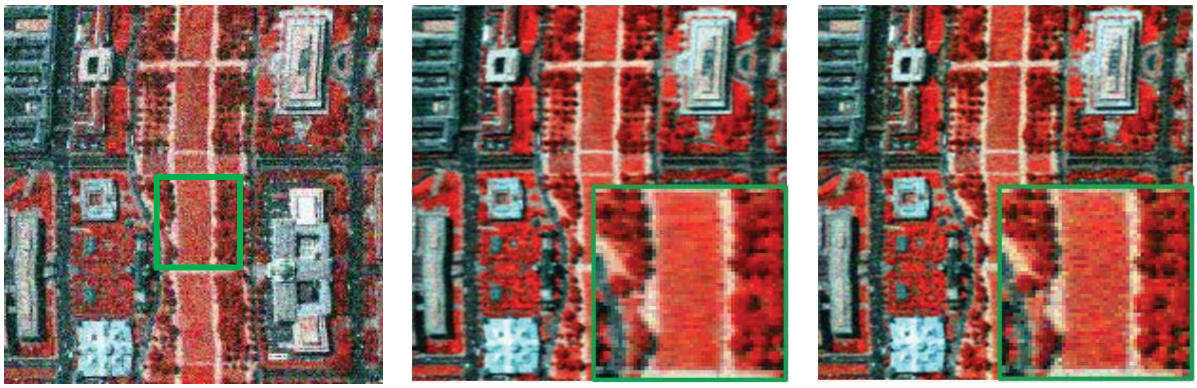

(a) (b) (c)

Fig. 6. Comparison between (4) and (5) for the spectral view denoising. (a) Noisy hyperspectral image. (b) Denoising with (4) for the spectral view (mean PSNR = 29.86, mean SSIM = 0.8755). (c) Denoising with (5) for the spectral view (mean PSNR = 29.35, mean SSIM = 0.8556).

the noise intensity in the different bands is similar. For the spatial view, it has been proved in [16] that the spectral–spatial adaptive model proposed in (5) is the better denoising method. However, for the spectral view, because it is different from the spatial view, the question is which is the better denoising model, (4) or (5). In the following, we give an example to discuss this issue.

The two models in (4) and (5) are both tested on the simulated noisy hyperspectral image, and the results are shown in Fig. 6. It can be seen that the model in (4) works better than the model in (5) for the spectral view, which is the opposite of the results for the spatial view. Therefore, the spectral view is denoised with model (4). We think the reason for this is that there is little spatial information in the spectral view, and the spatial information weighting process is therefore not necessary.

From the discussion above, the denoising models for the spatial and spectral views can be summarized as follows.

Spatial view denoising

$$\hat{u}^{\text{spa}} = \arg\min \left\{ \sum_{j=1}^{B} \left\| u_j^{\text{spa}} - f_j^{\text{spa}} \right\|_2^2 + \lambda \sum_{i=1}^{MN} W_i \sqrt{\sum_{j=1}^{B} (\nabla_{ij} u^{\text{spa}})^2} \right\}. \quad (7)$$

Spectral view denoising

$$\hat{u}^{\text{spe}} = \arg\min \left\{ \sum_{j=1}^{B} \left\| u_j^{\text{spe}} - f_j^{\text{spe}} \right\|_2^2 + \lambda \sum_{i=1}^{MN} \sqrt{\sum_{j=1}^{B} (\nabla_{ij} u^{\text{spe}})^2} \right\}. \quad (8)$$

In the two equations, u^{spa} and f^{spa} are the clear and noisy images in the spatial views, u^{spe} and f^{spe} are the clear and noisy images in the spectral views, B is the band number, and j means the jth band. The two models are both optimized with the split Bregman method in [16], which will be introduced as follows:

For (7), the data fidelity item can be rewritten as

$$\sum_{j=1}^{B} \left\| u_j^{\text{spa}} - f_j^{\text{spa}} \right\|_2^2 = \left\| u^{\text{spa}} - f^{\text{spa}} \right\|_2^2. \quad (9)$$

First, an auxiliary variable d is added instead ∇u^{spa} in (7)

$$\hat{u}^{\text{spa}} = \arg\min \left\{ \left\| u^{\text{spa}} - f^{\text{spa}} \right\|_2^2 + \lambda \sum_{i=1}^{MN} W_i \sqrt{\sum_{j=1}^{B} (d_{ij})^2} \right\} \quad \text{subject to } d = \nabla u^{\text{spa}}. \quad (10)$$

With the Bregman iteration [27], (10) can be changed into an unconstrained problem as follows:

$$\hat{u}^{\text{spa}} = \arg\min \left\{ \left\| u^{\text{spa}} - f^{\text{spa}} \right\|_2^2 + \lambda \sum_{i=1}^{MN} W_i \sqrt{\sum_{j=1}^{B} (d_{ij})^2} + \beta \left\| d - \nabla u^{\text{spa}} - b \right\|_2^2 \right\}. \quad (11)$$

In (11), b is also an auxiliary variable to accelerate the iteration. The minimization of (11) can be performed alternately with the following two subproblems:

subproblem u^{spa} :

$$\hat{u}^{\text{spa}} = \arg\min \left\{ \left\| u^{\text{spa}} - f^{\text{spa}} \right\|_2^2 + \beta \left\| d - \nabla u^{\text{spa}} - b \right\|_2^2 \right\} \quad (12)$$

subproblem d :

$$\hat{d} = \arg\min \left\{ \lambda \sum_{i=1}^{MN} W_i \sqrt{\sum_{j=1}^{B} (d_{ij})^2} + \beta \left\| d - \nabla u^{\text{spa}} - b \right\|_2^2 \right\}. \quad (13)$$

To solve two subproblems, the following equations must be solved:

$$(I - \beta\Delta) u_{k+1}^{\text{spa}} = f + \beta \nabla^T (d - b) \quad (14)$$

$$d = \text{shrink}\left(\sqrt{\sum_{j=1}^{B} (\nabla_{ij} u_{k+1}^{\text{spa}} + b_{k+1})^2}, \frac{\lambda W}{\beta} \right) \quad (15)$$

$$b_{k+1} = b_k + (\nabla u_{k+1}^{\text{spa}} - d_{k+1}) \quad (16)$$

where k is the iteration time, and the *shrink* operator stands for the soft thresholding process. Equation (14), because it is strictly diagonal, can be efficiently solved using the Gauss–Seidel iteration algorithm. The advantage of the split Bregman method is that the difficult optimization problem in (7) is split into the above two subproblems, which are very easy to optimize. The optimization of (8) is very similar to that of (7), except that the matrix W is removed.

Next, we analyze whether the denoising results from the two views are complementary to each other.

B. Analysis of the Complementary Nature of Spatial and Spectral View Denoising

In the following, we present an example to illustrate the complementary nature of the spatial and spectral view denoising results. In Fig. 7, with the Washington, DC Mall hyperspectral data as an example, the denoising results using (7) and (8), from both the spatial and spectral views, are presented. More details of the data are given in the experimental section. In Fig. 7, the first column is the original image, and the second column is the noisy image with a noise variance of 0.05 (the dynamic range of the image is normalized to 0–1). The denoising results from the spatial and spectral views are shown in the third and fourth columns, respectively. The second row presents a detailed part of the denoising results, the third row shows the denoising result in the spectral view, and the fourth row shows the spectral curve of the denoising result. From the comparison, it can be seen in the spatial view denoising result [Fig. 7(c)] that the edge and spatial information is well preserved, but the noise in the spectral dimension is not well suppressed, and some noise can still be clearly seen in the spectral curve. In the spectral view denoising result [Fig. 7(d)], the noise in the spectral dimension is well suppressed, and the spectral curve is more similar to the original image [Fig. 7(a)], but the spatial information appears blurred and some detailed information is lost. This suggests that the denoising results from the two views can complement each other, and fusing them could potentially improve the denoising result. Consequently, in the following section, we propose a metric Q-weighting strategy to fuse the denoising results of the spatial view and the spectral view.

C. Spatial–Spectral View Fusion Strategy

1) Blind Image Quality Metric Q: From the above analysis, it is seen that the denoising results from the spatial and spectral views can complement each other. Therefore, the next critical problem is how to fuse the two denoising results together. First, for each band, we must identify which one is the better of the two denoising results.

In this paper, the blind image quality evaluation index, named the metric Q and as proposed in [28], is adopted. The definition of the metric Q is as follows:

$$Q = s_1 \frac{s_1 - s_2}{s_1 + s_2} \quad (17)$$

where s_1 and s_2 are, respectively, the singular values of the gradient matrix G over an $N \times N$ window (w_i), and G has the following definition:

$$G = \begin{bmatrix} \vdots & \vdots \\ p_x(k) & p_y(k) \\ \vdots & \vdots \end{bmatrix} \quad k \in w_i \quad (18)$$

where k denotes the kth pixel in the window w_i. The metric Q is correlated with the noise level, sharpness, and intensity contrast of the structured regions of an image; it does not require any prior knowledge [28], and it is an effective blind image quality evaluation index. The larger the metric Q, the better the image quality. Therefore, for the two denoising results of each band, the metric Q value is calculated, and the two denoising results are fused with a metric Q weighting strategy.

2) Metric Q-Weighted Fusion Method: Let $\hat{u}^{\text{spa}} = [\hat{u}_1^{\text{spa}}, \hat{u}_2^{\text{spa}}, \hat{u}_3^{\text{spa}}, \ldots, \hat{u}_B^{\text{spa}}]$ be the denoising result of the spatial view, $\hat{u}^{\text{spe}} = [\hat{u}_1^{\text{spe}}, \hat{u}_2^{\text{spe}}, \hat{u}_3^{\text{spe}}, \ldots, \hat{u}_B^{\text{spe}}]$ is the denoising result of the spectral view, and B is the band number. For $\hat{u}^{\text{spa}}$ and $\hat{u}^{\text{spe}}$, we first compute the value of the metric Q of each band, respectively, which can be expressed as

$$Q^{\text{spa}} = \left[Q_1^{\text{spa}}, Q_2^{\text{spa}}, Q_3^{\text{spa}}, \ldots, Q_B^{\text{spa}} \right] \quad (19)$$

$$Q^{\text{spe}} = \left[Q_1^{\text{spe}}, Q_2^{\text{spe}}, Q_3^{\text{spe}}, \ldots, Q_B^{\text{spe}} \right]. \quad (20)$$

The final denoising result is then obtained by applying the metric Q weighted fusion strategy to the two denoising results

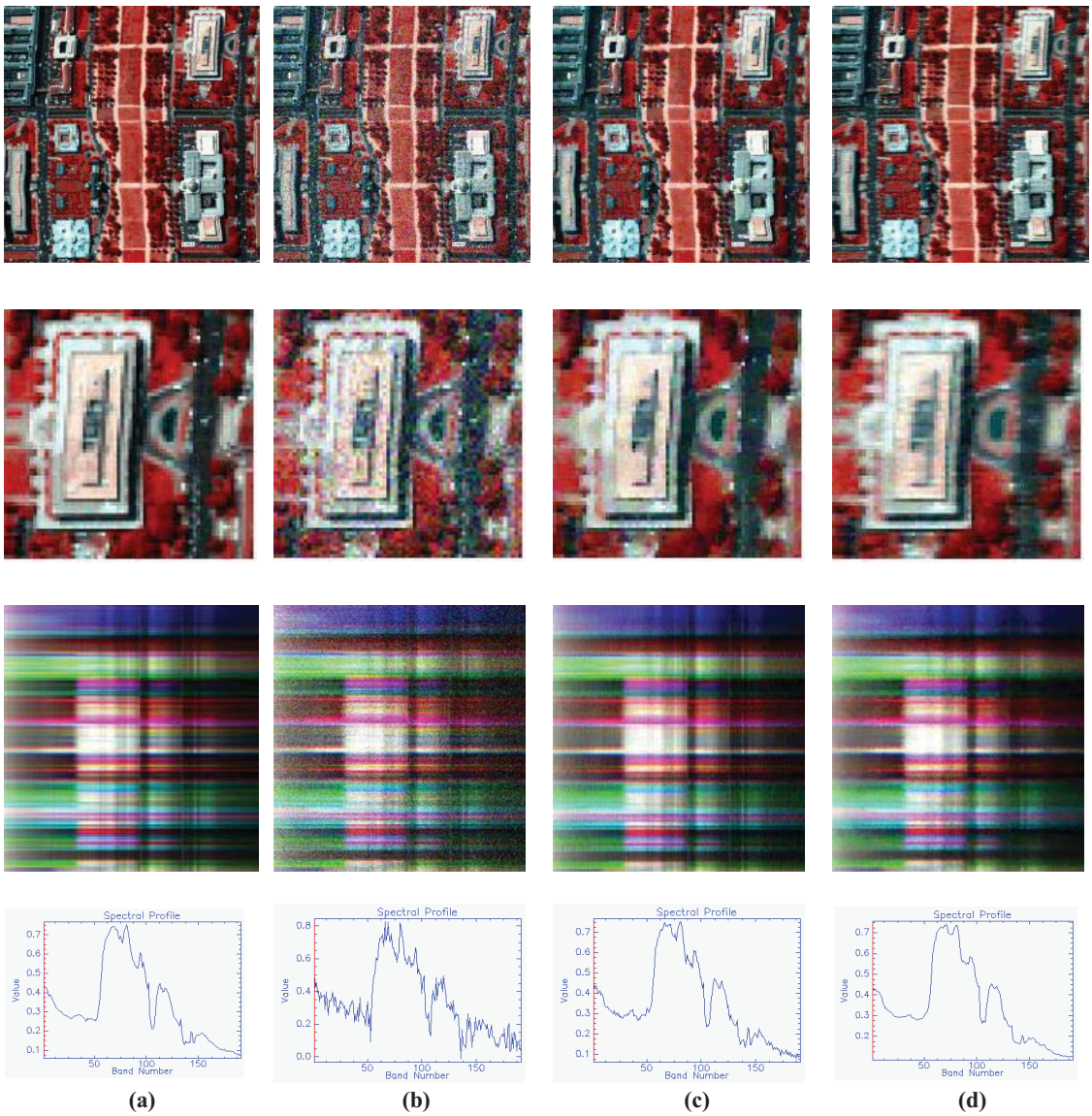

Fig. 7. Comparison between the spatial view and spectral view denoising results. (a) Original image. (b) Noisy image with a noise variance of 0.05. (c) Spatial view denoising result. (d) Spectral view denoising result.

of the different views, which can be expressed as

$$\hat{u}_j = \frac{Q_j^{\text{spa}} \hat{u}_j^{\text{spa}} + Q_j^{\text{spe}} \hat{u}_j^{\text{spe}}}{Q_j^{\text{spa}} + Q_j^{\text{spe}}}. \tag{21}$$

It is shown that the two denoising results are fused band by band.

IV. Experimental Results and Discussion

A. Simulated Experiment

In this section, the HYDICE image of the Washington, DC Mall, with a size of $200 \times 200 \times 191$, is used to verify the performance of the proposed algorithm. The experimental data were provided by Prof. David Landgrebe, and can be downloaded from [29]. Before the simulated process, the gray values of the hyperspectral image were normalized to between 0 and 1. The peak signal-to-noise ratio (PSNR) index and the structural similarity index (SSIM), as proposed in [30], are used to give a quantitative assessment of the results of the simulated experiments. For the hyperspectral image, we compute the PSNR and SSIM values between each clear band and denoised band, and then average them. These are denoted as MPSNR (mean peak signal-to-noise ratio) and MSSIM (mean structural similarity index). In order to evaluate the spectral fidelity of the denoising result, the mean spectral angle (MSA) index is also used.

In our method, the regularization parameter λ in (7) and (8) is adjusted until the best result is arrived at for both the spatial and spectral views. In the simulation experiments, the optimal λ is selected as the one with the highest mean PSNR and SSIM values.

For the simulated process, we simulate the addition of noise in the following two cases:

Case 1: For different bands, the noise intensity is equal: in this case, the same distribution of zero-mean Gaussian noise

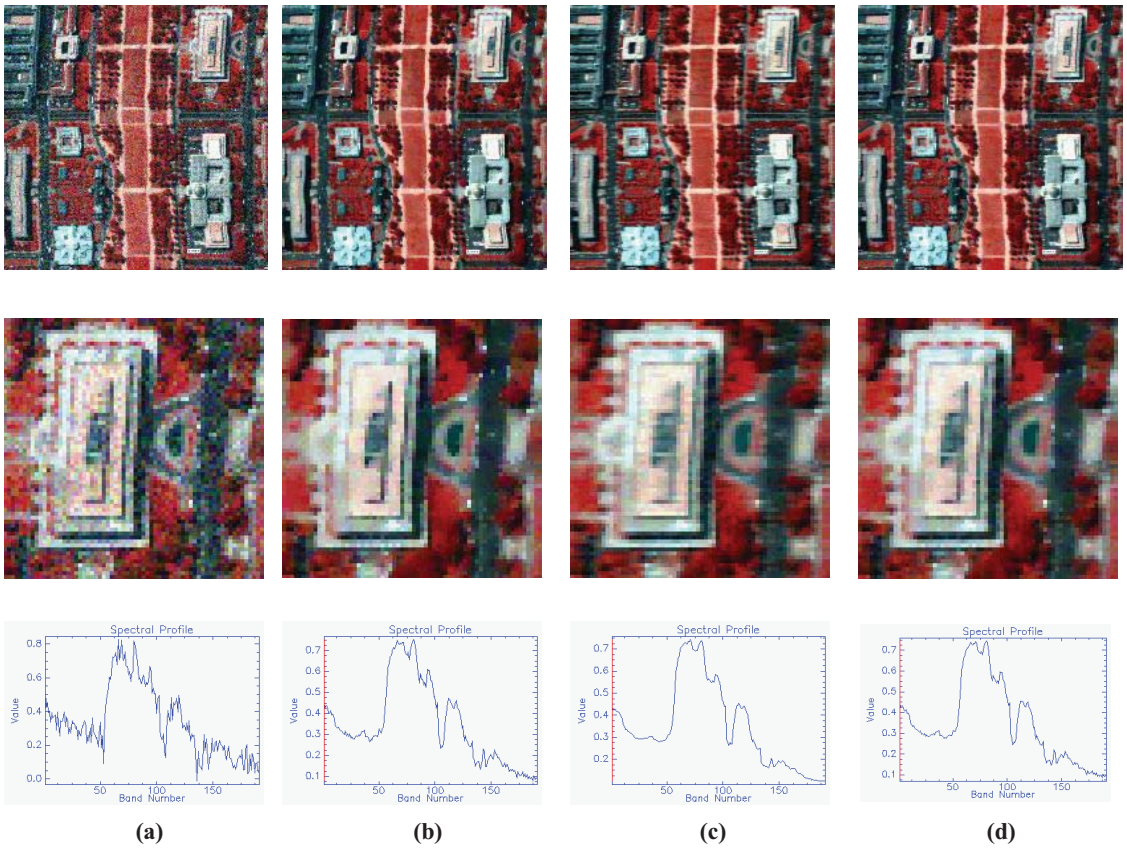

Fig. 8. Comparison between spatial view denoising, spectral view denoising, and the spatial-spectral view fusion results in simulated experiment 1. (a) Noisy image with a noise variance of 0.05. (b) Spatial view denoising result. (c) Spectral view denoising result. (d) Spatial and spectral view fusion result.

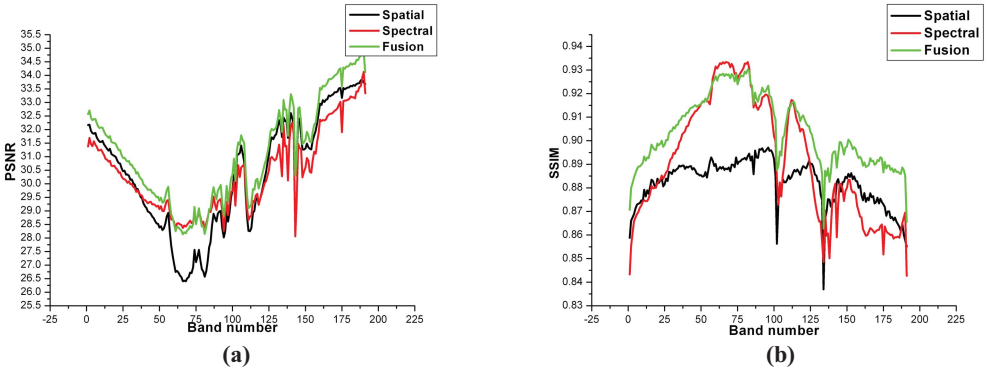

Fig. 9. Change in PSNR and SSIM values of the different bands before and after fusion in simulated experiment 1 (noise variance = 0.05). (a) PSNR value change. (b) SSIM value change.

is added to each band, with a variance of 0.02, 0.03, 0.05, 0.07, and 0.1.

Case 2: For different bands, the noise intensity is different: in this case, different variance zero-mean Gaussian noise is added to each band, the variance value being randomly selected from 0 to 0.05, and from 0 to 0.01.

Fig. 8 shows the denoising result of the 0.05 noise variance case. The quantitative evaluation of the denoising result is presented in Fig. 9 and Table I. Fig. 9 shows the changes in the PSNR and SSIM values of the different bands before and after fusion, and Fig. 10 gives the max, min, and mean of the PSNR and SSIM values in Fig. 9. In Table I, the MPSNR and MSSIM values of all the noise conditions are presented.

It can be seen that the proposed spatial–spectral view fusion denoising result is better than both the individual spatial view and spectral view denoising results. In the spatial view denoising result, although the spatial information is preserved well, the noise in the spectral dimension is not completely suppressed, and some noise still remains in the spectral curve. For the spectral view denoising result, the noise in the spectral dimension is suppressed well, and the spectral curve is very similar to the true spectral curve shown in Fig. 7(a), but in the spatial dimension the edges are blurred and the spatial information is not well preserved. For our spatial–spectral view fusion method, as the denoising results in the different views complement each other, the result is better than both the

TABLE I
QUANTITATIVE EVALUATION OF THE DENOISING RESULTS IN SIMULATED EXPERIMENT CASE 1

Noise Variance	Evaluation Index	Spatial View	Spectral View	**Fusion**
0.02	MPSNR	35.55	35.20	**36.21**
	MSSIM	0.9606	0.9582	**0.9669**
	MSA	2.91	3.06	**2.73**
	Time (s)	61.53	57.68	**88.84**
0.03	MPSNR	33.47	33.36	**34.14**
	MSSIM	0.9390	0.9400	**0.9486**
	MSA	3.77	3.93	**3.59**
	Time (s)	85.77	76.44	**81.43**
0.05	MPSNR	30.40	30.41	**31.12**
	MSSIM	0.8827	0.8917	**0.9040**
	MSA	5.02	5.01	**4.62**
	Time (s)	141.87	143.15	**82.42**
0.07	MPSNR	27.64	27.66	**28.23**
	MSSIM	0.7804	0.8153	**0.8247**
	MSA	6.27	5.86	**5.57**
	Time (s)	270.86	259.28	**86.08**
0.1	MPSNR	26.99	27.47	**27.85**
	MSSIM	0.7632	0.8046	**0.8124**
	MSA	7.13	6.78	**6.40**
	Time (s)	278.695	268.716	**77.303**

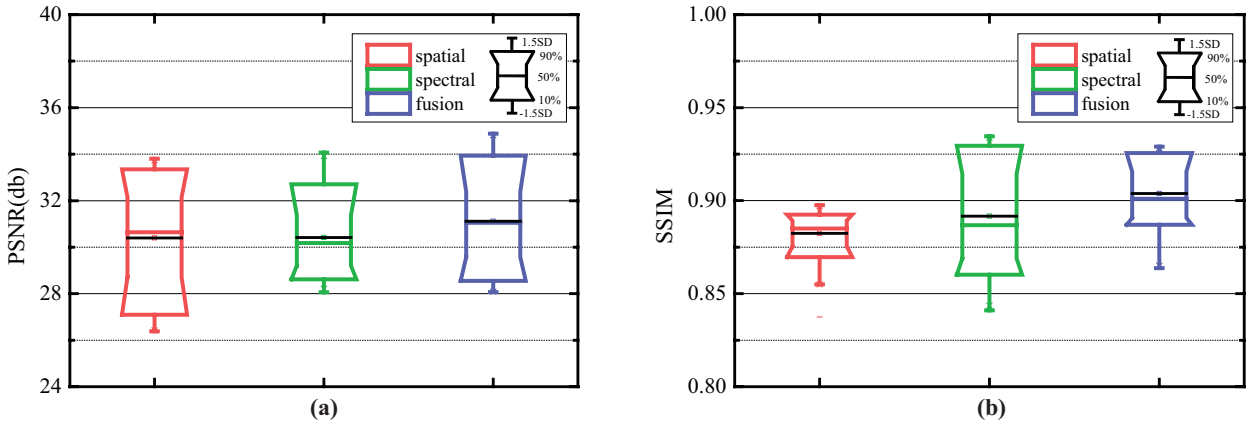

Fig. 10. Max, min, and mean of the PSNR and SSIM values in Fig. 9. (a) PSNR value. (b) SSIM value.

individual spatial view and spectral view denoising results. Not only is the spatial information well preserved but the noise in the spectral dimension is also better suppressed. The better performance of our method can also be seen in the quantitative evaluation results in Fig. 9 and Table I, where the PSNR and SSIM values are improved in almost all the bands after the denoising results of the two views are fused together. The proposed method also produces the highest MPSNR and MSSIM values, which illustrates the improved spatial information preservation property. Meanwhile, the MSA value of our method is the lowest, which reflects a better spectral fidelity. In addition, the result of the proposed fusion method is robust with the change of the noise intensity.

The denoising result of simulated case 2 is shown in Fig. 11, and the quantitative evaluation results are presented in Table II and Fig. 12. It can again be seen that the denoising result after fusion appears better than the single-view denoising results, both from the visual and quantitative aspects, when various noise intensities are distributed in the different bands. As described in Section III-A, when different intensity noise is added in the different bands, the noise distribution will appear different in the spatial and spectral views. In the spatial view, the noise intensity will vary in each band, while in the spectral view the noise intensity in each band will be similar. The experimental results in this case illustrate that the proposed hyperspectral TV model can deal with the two different noise conditions. For instance, for the spatial view, the hyperspectral TV model will give different denoising strengths to the different bands, while for the spectral view the

TABLE II
QUANTITATIVE EVALUATION OF THE DENOISING RESULTS IN SIMULATED EXPERIMENT CASE 2

Noise Variance	Evaluation Index	Spatial View	Spectral View	**Fusion**
0.05	MPSNR	34.03	33.44	**34.43**
	MSSIM	0.9415	0.9409	**0.9493**
	MSA	3.73	3.89	**3.58**
	Times (s)	75.54	65.09	**94.36**
0.1	MPSNR	30.14	29.85	**30.61**
	MSSIM	0.8711	0.8755	**0.8883**
	MSA	5.63	5.79	**5.38**
	Time (s)	146.17	128.79	**90.99**

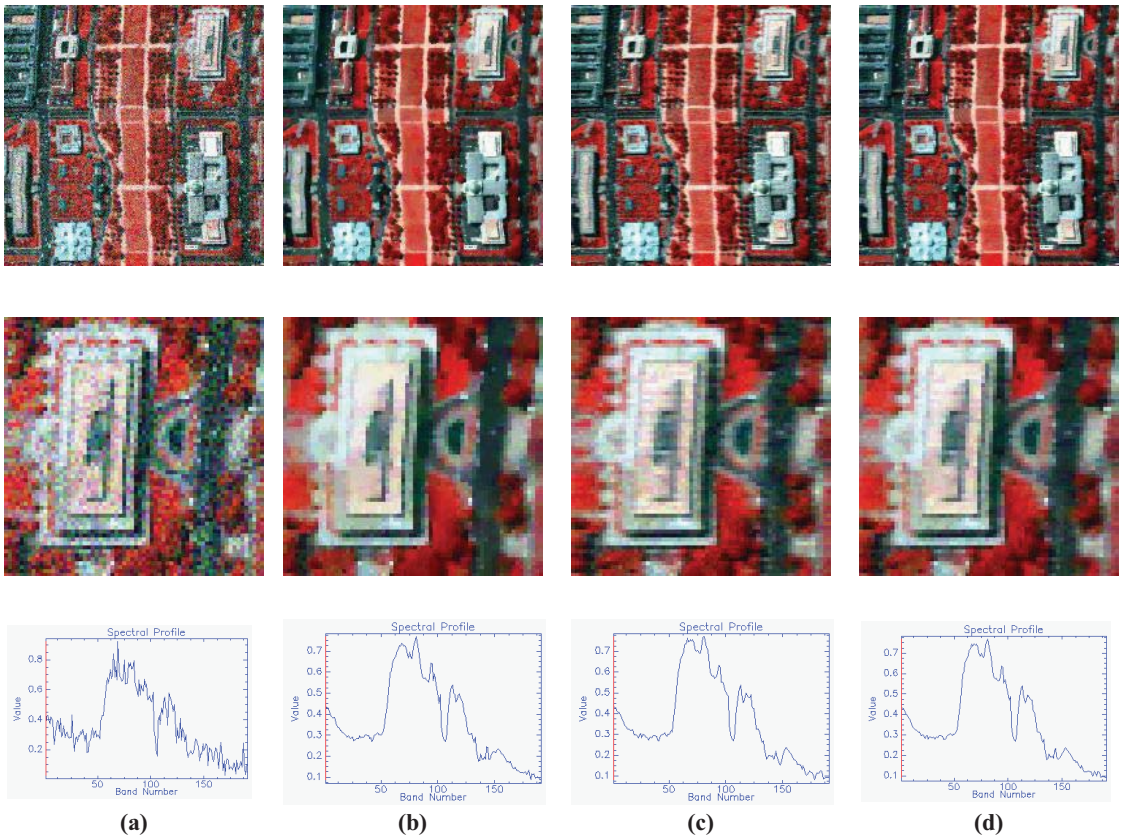

Fig. 11. Comparison between the spatial view denoising, spectral view denoising, and the spatial–spectral view fusion results in simulated case 2. (a) Noisy image. (b) Spatial view denoising result. (c) Spectral view denoising result. (d) Spatial–spectral view fusion result.

model will give a similar denoising strength to all the bands. These "spectrally adaptive" properties can guarantee a balance between "noise suppression" and "detail preservation."

B. Real Data Experiment

To further confirm the effectiveness of the proposed method, we also test it in a real data experiment. The HYDICE urban image [31] is selected as the real data, which has a size of 200×200 pixels and 205 bands. There is considerable high-intensity striping and mixed noise bands included in the data, examples of which are presented in column 1 of Fig. 13(a). In the real data experiment, the optimal λ is selected as the one with the highest Q value [28]. From the experimental result, it can be seen that, in the spatial view denoising result, although the high-intensity noise is well suppressed and the edges are well preserved, some textural information is over-smoothed, which can be clearly seen in the local detailed information presented in the last two rows of Fig. 13(b). In the spectral view denoising result presented in Fig. 13(c), not only is the noise not completely suppressed but the edge information also appears blurred. However, in the spectral view denoising result, the textural information is well preserved. Therefore, the denoising results of the two views can still complement each other, and after the denoising results of the two views are fused, the noise is well suppressed and, also, the detailed information, both in edges and textures, is well preserved.

TABLE III
QUANTITATIVE EVALUATION OF THE DENOISING RESULTS WHEN THE SPECTRAL–SPATIAL FUSION IDEA IS USED ON THE WIENER FILTER METHOD

Noise Variance	Evaluation Index	Spatial View	Spectral View	**Fusion**
0.02	MPSNR	30.58	29.34	**30.61**
	MSSIM	0.8739	0.8559	**0.8844**
	MSA	4.32	4.78	**4.10**
0.05	MPSNR	28.61	28.37	**29.38**
	MSSIM	0.8257	0.8296	**0.8585**
	MSA	6.19	5.88	**5.27**
0.1	MPSNR	25.35	26.54	**27.10**
	MSSIM	0.6967	0.7626	**0.7845**
	MSA	10.12	8.10	**7.74**

C. Discussion

In this paper, the hyperspectral TV model is used as the hyperspectral image denoising method. However, can this spatial and spectral fusion method still work with other denoising methods? To answer this question, we tested the spatial–spectral fusion idea with the adaptive Wiener filter [16], [32], and the evaluation results are shown in Table III, From the results, it is seen that for the simple spatially adaptive Wiener filter method, our proposed spatial and spectral fusion method still gives better results than the single-view denoising results, which illustrates that the fusion process is independent of the method used. Therefore, in future

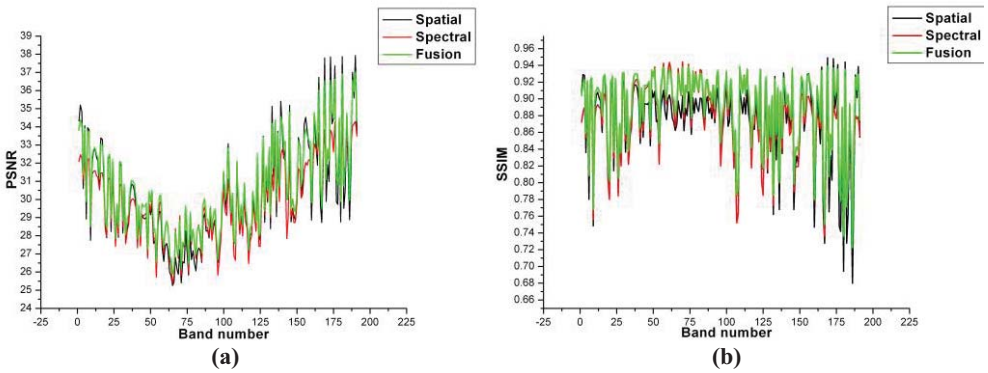

Fig. 12. Change in PSNR and SSIM values of the different bands before and after fusion in simulated experiment case 2. (a) PSNR value change. (b) SSIM value change.

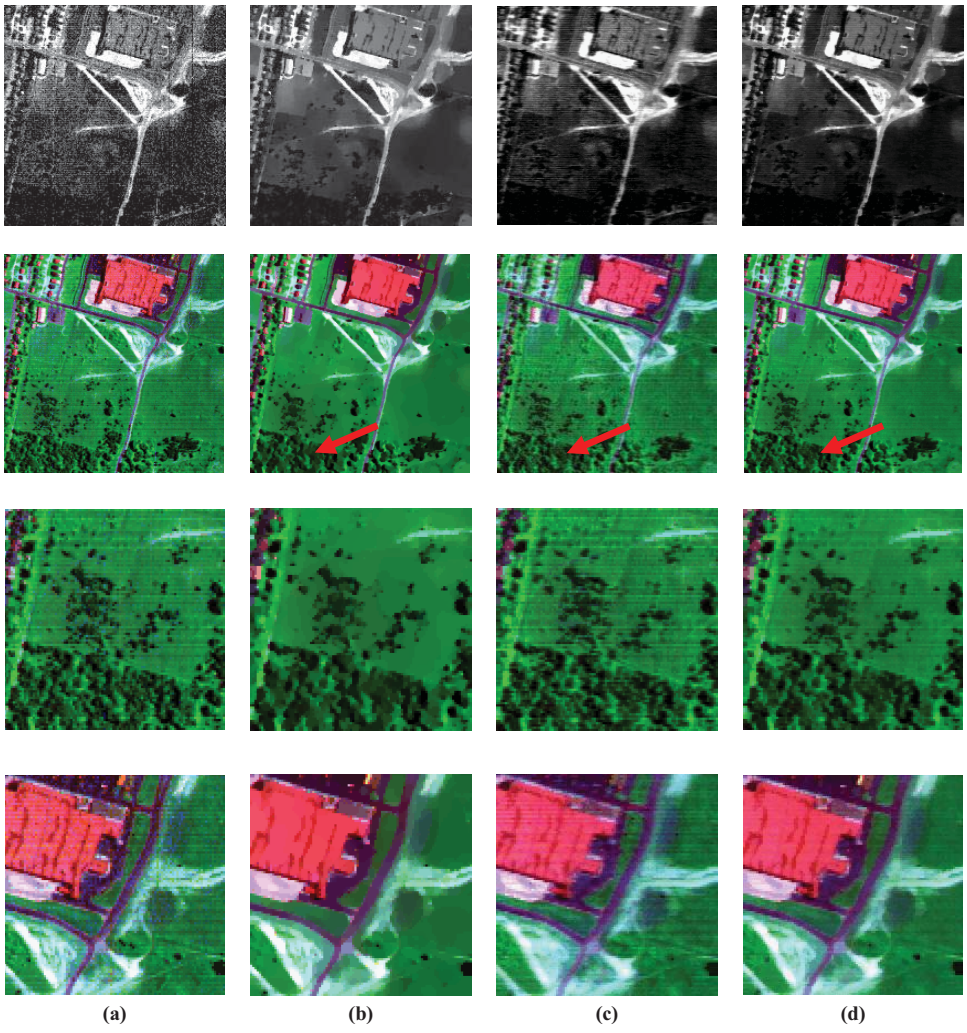

Fig. 13. Comparison between spatial view denoising, spectral view denoising, and the spatial-spectral view fusion results with real data. (a) Original noisy image. (b) Spatial view denoising result. (c) Spectral view denoising result. (d) Spatial–spectral view fusion result.

research, it will be interesting to try the spatial–spectral fusion idea on some other hyperspectral image denoising methods.

V. Conclusion

In this paper, a spatial–spectral view fusion method was proposed to denoise hyperspectral imagery. The original hyperspectral image was first denoised with a hyperspectral total variation method, from both the spatial and spectral views, and then the denoising results of the two views were fused together with a Q-weighting strategy. The experimental results indicated that the proposed spatial–spectral view fusion method produces better denoising results than both the individual spatial view and spectral view denoising methods.

However, the proposed fusion idea could still be further improved in certain aspects. For example, in this paper we assumed that the noise was independent of the clear hyperspectral signal, while the signal-dependent noise characteristic of hyperspectral imagery has recently been discussed [33]–[36]. How to extend the hyperspectral TV model and spatial–spectral fusion idea to a signal-dependent noise type will be very interesting. In addition, the adaptive selection of the regularization parameter λ will be in our future research agenda.

ACKNOWLEDGMENT

The authors would like to thank Prof. D. Landgrebe, Purdue University, for providing the free downloads of the HYDICE image of the Washington, DC Mall test data, and also the handling editor and anonymous reviewers for their careful reading and helpful remarks. Dr. Q. Yuan would like to dedicate this paper to his mother, in memory of her eternal love.

REFERENCES

[1] C.-I. Chang, *Hyperspectral Data Exploitation: Theory and Applications*. Chichester, U.K.: Blackwell, 2007.
[2] A. Plaza, J. A. Benediktsson, J. W. Boardman, J. Brazile, L. Bruzzone, G. Camps-Valls, J. Chanussot, M. Fauvel, P. Gamba, A. Gualtieri, M. Marconcini, J. C. Tilton, and G. Trianni, "Recent advances in techniques for hyperspectral image processing," *Remote Sens. Environ.*, vol. 113, pp. S110–S122, Sep. 2009.
[3] J. M. Bioucas-Dias and J. M. P. Nascimento, "Hyperspectral subspace identification," *IEEE Trans. Geosci. Remote Sens.*, vol. 46, no. 8, pp. 2435–2445, Aug. 2008.
[4] O. Kuybeda, D. Malah, and M. Barzohar, "Rank estimation and redundancy reduction of high dimensional noisy signals with preservation of rare vectors," *IEEE Trans. Signal Process.*, vol. 55, no. 12, pp. 5579–5592, Dec. 2007.
[5] N. Acito, M. Diani, and G. Corsini, "Hyperspectral signal subspace identification in the presence of rare signal components," *IEEE Trans. Geosci. Remote Sens.*, vol. 48, no. 4, pp. 1940–1954, Apr. 2010.
[6] H. Othman and S. Qian, "Noise reduction of hyperspectral imagery using hybrid spatial-spectral derivative-domain wavelet shrinkage," *IEEE Trans. Geosci. Remote Sens.*, vol. 44, no. 2, pp. 397–408, Feb. 2006.
[7] G. Chen, S. Qian, and W. Xie, "Denoising of hyperspectral imagery using principal component analysis and wavelet shrinkage," *IEEE Trans. Geosci. Remote Sens.*, vol. 49, no. 3, pp. 973–980, Mar. 2011.
[8] D. Letexier and S. Bourennane, "Noise removal from hyperspectral images by multidimensional filtering," *IEEE Trans. Geosci. Remote Sens.*, vol. 46, no. 7, pp. 2061–2069, Jul. 2008.
[9] X. Liu, S. Bourennane, and C. Fossati, "Denoising of hyperspectral images using the PARAFAC model and statistical performance analysis," *IEEE Trans. Geosci. Remote Sens.*, vol. 50, no. 10, pp. 3717–3724, Oct. 2012.
[10] A. Karami, M. Yazdi, and A. Z. Asli, "Noise reduction of hyperspectral images using kernel non-negative tucker decomposition," *IEEE J. Sel. Topics Signal Process.*, vol. 5, no. 3, pp. 487–493, Jun. 2011.
[11] D. Letexier, S. Bourennane, and B. Talon, "Nonorthogonal tensor matricization for hyperspectral image filtering," *IEEE Geosci. Remote Sens. Lett.*, vol. 5, no. 1, pp. 3–7, Jan. 2008.
[12] J. Martin-Herrero, "Anisotropic diffusion in the hypercube," *IEEE Trans. Geosci. Remote Sens.*, vol. 45, no. 5, pp. 1386–1398, May 2007.
[13] R. Mendez-Rial and J. Martin-Herrero, "Efficiency of semi-implicit schemes for anisotropic diffusion in the hypercube," *IEEE Trans. Image Process.*, vol. 21, no. 5, pp. 2389–2398, May 2012.
[14] Y. Wang, R. Niu, and X. Yu, "Anisotropic diffusion for hyperspectral imagery enhancement," *IEEE Sensors J.*, vol. 10, no. 3, pp. 469–477, Mar. 2010.
[15] P. Liu, F. Huang, G. Li, and Z. Liu, "Remote-sensing image denoising using partial differential equations and auxiliary images as priors," *IEEE Geosci. Remote Sens. Lett.*, vol. 9, no. 3, pp. 358–362, May 2012.
[16] Q. Yuan, L. Zhang, and H. Shen, "Hyperspectral image denoising employing a spectral-spatial adaptive total variation model," *IEEE Trans. Geosci. Remote Sens.*, vol. 50, no. 10, pp. 3660–3677, Oct. 2012.
[17] T. Poggio, V. Torre, and C. Koch, "Computational vision and regularization theory," *Nature*, vol. 317, no. 6035, pp. 314–319, 1985.
[18] X. Wang, D. Tao, and Z. Li, "Entropy controlled Laplacian regularization for least square regression," *Signal Process.*, vol. 90, no. 6, pp. 2043–2049, 2010.
[19] C. Bouman and K. Sauer, "A generalized Gaussian image model for edge-preserving MAP estimation," *IEEE Trans. Image Process.*, vol. 2, no. 3, pp. 296–310, Jul. 1993.
[20] L. Rudin, S. Osher, and E. Fatemi, "Nonlinear total variation based noise removal algorithms," *Phys. D*, vol. 60, nos. 1–4, pp. 259–268, Nov. 1992.
[21] B. Geng, D. Tao, C. Xu, Y. Yang, and X. Hua, "Ensemble manifold regularization," *IEEE Trans. Pattern Anal. Mach. Intell.*, vol. 34, no. 6, pp. 1227–1233, Jun. 2012.
[22] S. Si, D. Tao, and B. Geng, "Bregman divergence-based regularization for transfer subspace learning," *IEEE Trans. Knowl. Data Eng.*, vol. 22, no. 7, pp. 929–942, Jul. 2010.
[23] J. Oliveira, J. Bioucas-Dias, and M. Figueiredo, "Adaptive total variation image deblurring: A majorization-minimization approach," *Signal Process.*, vol. 89, no. 9, pp. 1683–1693, 2009.
[24] M. Ng, H. Shen, E. Lam, and L. Zhang, "A total variation regularization based super-resolution reconstruction algorithm for digital video," *EURASIP J. Adv. Signal Process.*, vol. 2007, no. 18, pp. 74585-1–74585-16, 2007.
[25] Q. Yuan, L. Zhang, and H. Shen, "Multiframe super-resolution employing a spatially weighted total variation model," *IEEE Trans. Circuits Systs. Video Technol.*, vol. 22, no. 3, pp. 379–392, Mar. 2012.
[26] A. Buades, T. M. Le, J. M. Morel, and L. A. Vese, "Fast cartoon + texture image filters," *IEEE Trans. Image Process.*, vol. 19, no. 8, pp. 1978–1986, Aug. 2010.
[27] T. Goldstein and S. Osher, "The split Bregman method for L1 regularized problems," *SIAM J. Imag. Sci.*, vol. 2, no. 2, pp. 323–343, May 2009.
[28] X. Zhu and P. Milanfar, "Automatic parameter selection for denoising algorithms using a no-reference measure of image content," *IEEE Trans. Image Process.*, vol. 19, no. 12, pp. 3116–3132, Dec. 2010.
[29] [Online]. Available: https://engineering.purdue.edu/~biehl/MultiSpec/hyperspectral.html
[30] Z. Wang, A. C. Bovik, and H. R. Sheikh, "Image quality assessment: From error visibility to structural similarity," *IEEE Trans. Image Process.*, vol. 13, no. 4, pp. 600–612, Apr. 2004.
[31] [Online]. Available: http://www.tec.army.mil/hypercube
[32] [Online]. Available:http://www.mathworks.cn/help/toolbox/images/ref/wiener2.html
[33] J. Meola, M. T. Eismann, R. L. Moses, and J. N. Ash, "Modeling and estimation of signal-dependent noise in hyperspectral imagery," *Appl. Opt.*, vol. 50, no. 21, pp. 3829–3846, 2011.
[34] N. Acito, M. Diani, and G. Corsini, "Signal-dependent noise modeling and model parameter estimation in hyperspectral images," *IEEE Trans. Geosci. Remote Sens.*, vol. 49, no. 8, pp. 2957–2971, Aug. 2011.
[35] M. L. Uss, B. Vozel, V. V. Lukin, and K. Chehdi, "Local signal-dependent noise variance estimation from hyperspectral textural images," *IEEE J. Sel. Topics Signal Process.*, vol. 5, no. 3, pp. 459–486, Jun. 2011.
[36] N. Acito, M. Diani, and G. Corsini, "Subspace-based striping noise reduction in hyperspectral images," *IEEE Trans. Geosci. Remote Sens.*, vol. 49, no. 4, pp. 1325–1342, Apr. 2011.

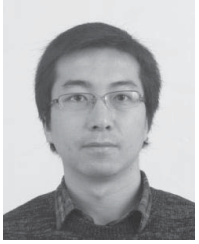

Qiangqiang Yuan received the B.S. degree in surveying and mapping engineering and the Ph.D. degree in photogrammetry and remote sensing from Wuhan University, Wuhan, China, in 2006 and 2012, respectively.

He joined the School of Geodesy and Geomatics, Wuhan University, in July 2012, where he is currently an Assistant Professor. His current research interests include image reconstruction, remote sensing image processing and application, data fusion and assimilation.

Dr. Yuan is a Reviewer of the IEEE TRANSACTIONS ON GEOSCIENCE AND REMOTE SENSING, the *ISPRS Journal of Photogrammetry and Remote Sensing*, and the IEEE SIGNAL PROCESSING LETTERS.

Liangpei Zhang (M'06–SM'08) received the B.S. degree in physics from Hunan Normal University, Changsha, China, in 1982, the M.S. degree in optics from the Xi'an Institute of Optics and Precision Mechanics, Chinese Academy of Sciences, Xi'an, China, in 1988, and the Ph.D. degree in photogrammetry and remote sensing from Wuhan University, Wuhan, China, in 1998.

He is currently the Head of the Remote Sensing Division, State Key Laboratory of Information Engineering, Surveying, Mapping, and Remote Sensing, Wuhan University. He is also a "Chang-Jiang Scholar" Chair Professor appointed by the Ministry of Education of China. He is currently a Principal Scientist for the China State Key Basic Research Project (2011–2016) appointed by the Ministry of National Science and Technology of China to lead the remote sensing program in China. He has authored more than 260 research papers. He holds five patents. His current research interests include hyperspectral remote sensing, high-resolution remote sensing, image processing, and artificial intelligence.

Dr. Zhang is a fellow of the IEE, Executive Member (Board of Governor) of the China National Committee of International Geosphere-Biosphere Programme, Executive Member of the China Society of Image and Graphics. He regularly serves as a General Chair of 4th IEEE Workshop on Hyperspectral Image and Signal Processing: Evolution in Remote Sensing (Whispers, 2012), Co-Chair of the series SPIE Conferences on Multispectral Image Processing and Pattern Recognition, Conference on Asia Remote Sensing, and many other conferences. He edits several conference proceedings, issues, and Geoinformatics Symposiums. He also serves as an Associate Editor of the IEEE TRANSACTIONS ON GEOSCIENCE AND REMOTE SENSING, the *International Journal of Ambient Computing and Intelligence*, the *International Journal of Image and Graphics*, the *International Journal of Digital Multimedia Broadcasting*, the *Journal of Geo-spatial Information Science*, and the *Journal of Remote Sensing*.

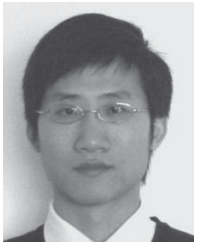

Huanfeng Shen (M'11–SM'13) received the B.S. degree in surveying and mapping engineering and the Ph.D. degree in photogrammetry and remote sensing from Wuhan University, Wuhan, China, in 2002 and 2007, respectively.

He joined the School of Resources and Environmental Science, Wuhan University, in July 2007, where he is currently a Full Professor. He has authored more than 60 research papers. His current research interests include image processing (for quality improvement), remote sensing application, data fusion, and assimilation. He has been supported by several talent programs, including the New Century Excellent Talents by the Ministry of Education of China in 2011 and the Hubei Science Fund for Distinguished Young Scholars in 2011.